Confronting spin flavor solutions of the solar neutrino problem with current and future solar neutrino data

J. Barranco,[1,*] O. G. Miranda,[1,†] T. I. Rashba,[2,‡] V. B. Semikoz,[2,§] and J. W. F. Valle[3,‖]
[1]*Departamento de Física, Centro de Investigación y de Estudios, Avanzados Apdo. Postal 14-740 07000 Mexico, DF, Mexico*
[2]*Institute of Terrestrial Magnetism, Ionosphere and Radio Wave Propagation of the Russian Academy of Sciences, 142190, Troitsk, Moscow Region, Russia*
[3]*Instituto de Física Corpuscular–CSIC, Universitat de València, Edificio Institutos, Apt. 22085, E-46071 València, Spain*
(Received 7 August 2002; published 27 November 2002)

A global analysis of spin flavor precession (SFP) solutions to the solar neutrino problem is given, taking into account the impact of the full set of latest solar neutrino data, including the recent SNO data and the 1496-day Super-Kamiokande data. These are characterized by three effective parameters: $\Delta m^2_{SOL} \equiv \Delta m^2$, the neutrino mixing angle $\theta_{SOL} \equiv \theta$, and the magnetic field parameter $\mu B_\perp$. For the last we adopt a self-consistent magnetohydrodynamics field profile in the convective zone and identify an optimum $B_\perp \sim 80$ kG strength for $\mu = 10^{-11}\mu_B$. We find that no low mass (LOW) quasivacuum or vacuum solutions are present at 3σ. In addition to the standard large mixing angle (LMA) oscillation solution, there are two SFP solutions, in the resonant (RSFP) and nonresonant (NRSFP) regimes. These two SFP solutions have a goodness of fit of 84% (RSFP) and 83% (NRSFP), slightly better than the LMA oscillation solution (78%). We discuss the role of solar antineutrino searches in the fit and present a table of best-fit parameters and $\chi^2_{\min}$ values. Should the KamLAND experiment confirm the LMA solution, the SFP solutions may at best be present at a subleading level, leading to a constraint on $\mu B_\perp$. In the event the LMA is not the solution realized in nature, then experiments such as Borexino can help in distinguishing the LMA solution from the NRSFP solution and the simplest RSFP solution with no mixing.

DOI: 10.1103/PhysRevD.66.093009 PACS number(s): 14.60.Pq, 13.15.+g, 26.65.+t

I. INTRODUCTION

The recent neutral current and day-night measurements at the Sudbury Neutrino Observatory (SNO) [1,2] as well as the 1496-day solar neutrino data from Super-Kamiokande [3] combined with previous solar neutrino data [4] have shed more light on the long-standing problem posed by the solar neutrino anomaly. Evidence from atmospheric neutrino data also indicates that atmospheric neutrino conversions take place [5] and involve mainly two flavors, in order to comply with combined constraints from reactor neutrinos [6].

While the oscillation interpretation of the atmospheric data is rather robust [7], present solar data are not yet enough to pin down the mechanism underlying the neutrino flux suppression. Although neutrino oscillations provide the most commonly analyzed solution to both solar and atmospheric anomalies [8,9] at least two alternative mechanisms based on nonstandard neutrino matter interactions [10] and neutrino spin flavor precession [11–15] have been considered.

In this paper we reconsider the status of two-flavor spin flavor precession (SFP) solutions of the solar neutrino anomaly. The latter require the existence of nonzero transition magnetic moments of neutrinos [16] and the interplay of matter effects [17]. On general grounds one can argue that, if present, neutrino magnetic moments should be of this type, as one expects neutrinos to be Majorana particles [18]. Such spin flavor precession conversions represent an attractive way of accounting for present solar neutrino data. Since they involve only active neutrinos,[1] these are actually the only magnetic-moment-type solutions that survive the evidence, e.g., from SNO neutral current (NC) data, that solar neutrinos do convert to *active* neutrino states, and have just the right features to reconcile the SNO charged current (CC) and Super-Kamiokande results. It has also been shown how such solutions are robust in the sense that the choice of the solar magnetic field profile in the convective zone can be made self-consistently. Following Refs. [11,12] we adopt as profiles the static magnetohydrodynamics solutions obtained by Kutvitskii and Solov'ev (KS) [19].

Here we examine the status of all solutions described by the general two-flavor spin flavor precession Hamiltonian, which include the oscillation solutions as a particular case. Using this generalized picture we show that both SFP solutions give very good descriptions of the totality of current solar neutrino data, slightly better than the best oscillation solution, namely, the large mixing angle (LMA) solution [20], now robustly preferred among the oscillation solutions [9,21–26]. For the best chosen magnetic field strength there are no vacuum or low mass (LOW) quasivacuum solutions at the 3σ level. However, in addition to the LMA solution, there are two SFP solutions, resonant and non-resonant, characterized by a goodness of fit 84% and 83%, respectively.

*Electronic address: jbarranc@fis.cinvestav.mx
†Electronic address: Omar.Miranda@fis.cinvestav.mx
‡Electronic address: rashba@izmiran.rssi.ru
§Electronic address: semikoz@orc.ru, semikoz@ific.uv.es
‖Electronic address: valle@ific.uv.es

[1]Transition magnetic moments to sterile neutrinos are rejected by the SNO neutral current data.

We present a table of best-fit values and $\chi^2_{\rm min}$ and discuss the role of electron antineutrinos from the sun [27–29] in the fit. The latter will play an even more important role in the future, should KamLAND confirm the LMA oscillation solution. In this case the SFP solution may be realized at best at subleading level, leading to a constraint on $\mu B_\perp$. This bound is complementary to bounds on neutrino magnetic moments, such as the one discussed in Ref. [30]. In the event this is not the solution realized in nature, then future experiments such as Borexino can help to distinguish between SFP and LMA solutions.

II. NEUTRINO EVOLUTION AND CONVERSIONS

The recent SNO data strongly support the idea that solar neutrinos convert to *active* neutrinos. On the other hand the combined constraints from reactor neutrino experiments [6] and atmospheric neutrino data [8] imply that solar neutrino conversions involve mainly two flavors.

Here we consider the evolution Hamiltonian describing a system of two flavors of active Majorana neutrinos first considered [16]:

$$i\begin{pmatrix}\dot{\nu}_{eL}\\ \dot{\bar{\nu}}_{eR}\\ \dot{\nu}_{\mu L}\\ \dot{\bar{\nu}}_{\mu R}\end{pmatrix} = \begin{pmatrix} V_e-c_2\delta & 0 & s_2\delta & \mu B_+(t)\\ 0 & -V_e-c_2\delta & -\mu B_-(t) & s_2\delta\\ s_2\delta & -\mu B_+(t) & V_\mu+c_2\delta & 0\\ \mu B_-(t) & s_2\delta & 0 & -V_\mu+c_2\delta\end{pmatrix} \times\begin{pmatrix}\nu_{eL}\\ \bar{\nu}_{eR}\\ \nu_{\mu L}\\ \bar{\nu}_{\mu R}\end{pmatrix}. \quad (1)$$

In Eq. (1) $c_2=\cos 2\theta$, $s_2=\sin 2\theta$, $\delta=\Delta m^2/4E$, assumed to be always positive are the neutrino oscillation parameters; μ is the neutrino transition magnetic moment; $B_\pm=B_x\pm iB_y$ are the magnetic field components orthogonal to the neutrino momentum; $V_e(t)=G_F\sqrt{2}[N_e(t)-N_n(t)/2]$ and $V_\mu(t)=G_F\sqrt{2}[-N_n(t)/2]$ are the neutrino vector potentials for ν_{eL} and $\nu_{\mu L}$ in the Sun, given by $N_e(t)$ and $N_n(t)$, the number densities of the electrons and neutrons, respectively. This generalized form takes into account that, in addition to mixing, massive Majorana neutrinos may be endowed with a nonzero transition magnetic moment. In the limit where $\mu B\to 0$ this system reduces to the widely discussed case of two-flavor oscillations. On the other hand when the mixing vanishes, $\sin 2\theta\to 0$, one recovers the pure magnetic solutions considered in [12–15]. As we will see, it will be important to take into account the effects of neutrino mixing in the characterization of the SFP solutions.

In our calculations of SFP neutrino survival probabilities we use the electron and neutron number densities from the Bahcall-Baso-Pinsonneault 2000 (BBP00) model [31] with the magnetic field profile obtained in Ref. [12] for $k=6$ and $R_0=0.6R_\odot$. Finally, in order to obtain Earth matter effects we integrate numerically the evolution equation in the Earth matter using the Earth density profile given in the preliminary reference Earth model [32].

The combined amplitude for a solar ν_e to be detected as ν_α (α being $e,\mu,\bar{e},\bar{\mu}$) with energy E at a detector in the Earth can be written as

$$A^{S\text{-}V\text{-}E}_{\nu_e\to\nu_\alpha}=\langle\nu_\alpha|U^{\rm Earth}U^{\rm Vacuum}U^{\rm Sun}|\nu_e\rangle = \sum_{i=1,2,1,2} A^S_{ei}A^E_{i\alpha}\exp[-im_i^2(L-R_\odot)/2E]. \quad (2)$$

Here A^S_{ei} is the amplitude of the transition $\nu_e\to\nu_i$ (ν_i is the i-mass eigenstate) from the production point to the Sun surface, $A^E_{i\alpha}$ is the amplitude of the transition $\nu_i\to\nu_\alpha$ from the Earth surface to the detector, and the propagation in vacuum from the Sun to the surface of the Earth is given by the exponential, where L is the distance between the center of the Sun and the surface of the Earth, and $R_\odot$ is the radius of the Sun. While the presence of a magnetic field couples the four states in the evolution, its absence in vacuum and in the Earth produces the decoupling of the four states into two doublets: (ν_e, ν_μ) and ($\bar{\nu_e}$, $\bar{\nu_\mu}$). The corresponding probabilities $P_{e\alpha}$ can be found by numerically solving the evolution equation (1). Note that in the limit $B_\perp\to 0$ we recover the oscillation case.

With the above we proceed to analyze the behavior of our neutrino survival probabilities with respect to variations in $\mu B_\perp$. For the simple case of constant matter density and field strength and neglecting Earth regeneration effects, this was given explicitly in Eq. (8) of Ref. [11]. The basic feature

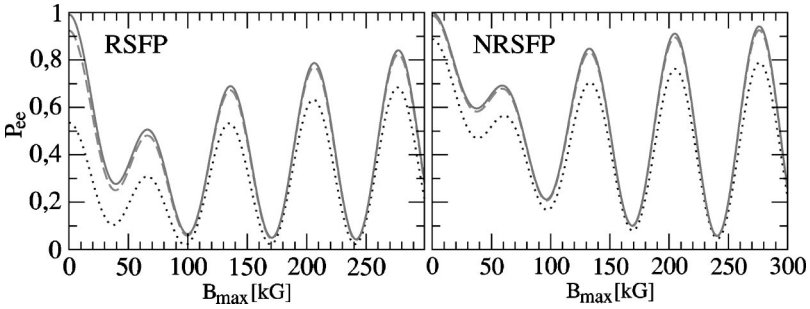

FIG. 1. Neutrino survival probabilities versus magnetic field strength ($B_{\rm max}$). The neutrino oscillation parameters have been fixed as $E/\Delta m^2=1.25\times 10^8$ MeV/eV^2, $\tan^2\theta=0.001$ (solid line), 0.01 (dashed line), and 0.1 (dotted line) in the left panel (''light'' side). The corresponding numbers for the ''dark'' side (right panel) are $E/\Delta m^2=2.5\times 10^8$ MeV/eV^2, $\tan^2\theta=10$ (dotted line), 100 (dashed line), and 1000 (solid line). Here we fix $\mu=10^{-11}\mu_B$.

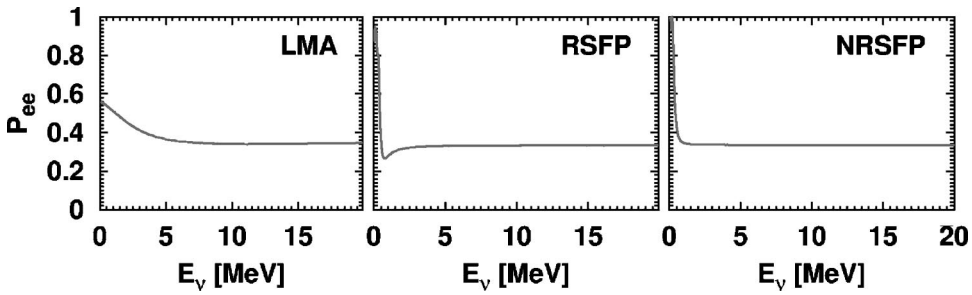

FIG. 2. Optimum two-neutrino survival probabilities for the LMA solution (left panel) and for the two SFP solutions: RSFP (middle panel) and NRSFP (right panel).

to note in this case is that the survival probability exhibits a periodic behavior. In Fig. 1 we show that such behavior also holds in the case of realistic matter density and magnetic field profiles obtained from magnetohydrodynamics [19]. One can see that, both for ''light'' side [resonant (R) RSFP-like] and ''dark'' side [nonresonant (NR) SFP-like] solutions the neutrino survival probabilities exhibit an approximately periodic behavior with respect to $\mu B_\perp$. Note that we have fixed a transition magnetic moment of $10^{-11}\mu_B$, consistent with existing present experiments. Examining Fig. 1 one sees that the smallest magnetic field magnitude that leads to a boron neutrino survival at the required level lies close to 80 kG. For simplicity, in what follows we will adopt the optimum strength $B_\perp \sim 80$ kG, because, being the smallest, it is probably the one preferred by astrophysics. It is straightforward to repeat our analysis for higher field strengths. This will lead to ''recurrences'' in solution space, i.e., to the existence of additional branches of the RSFP-like solutions, such as can be seen, for example, from Figs. 4 and 6 in Ref. [12]. Similarly, there will be additional branches of the ''basic'' NRSFP-like solution found in Ref. [11]. For simplicity we focus, in what follows, on the analysis of the ''first'' RSFP and NRSFP-like solutions, and their comparison with today's favorite oscillation solution, the LMA.

In Fig. 2 we show a schematic view of the spin flavor precession survival probabilities for both resonant and nonresonant cases, RSFP (middle panel), and NRSFP (right panel). The survival probabilities for the LMA case are also shown, for comparison, in the left panel. For the LMA case the neutrinos are converted into muon neutrinos, while for the SFP scenario the neutrinos are mainly converted into muon antineutrinos. Note that the above survival probabilities have been given for the best-fit parameter values determined in our fit (see Table I, below).

TABLE I. Best-fit values of Δm^2 and $\tan^2\theta$ with the corresponding $\chi^2_{\rm min}$ and GOF for the standard oscillation case (top panel) and for nonzero magnetic field (middle and bottom panels). The squared mass differences are given in $\rm eV^2$.

Region	$\tan^2\theta$	Δm^2	$\chi^2_{\rm min}$	GOF
	Standard oscillation			
LMA	0.47	5.6×10^{-5}	68.0	78%
	$\mu_\nu B\neq 0$ without SNO CC $\bar{\nu}_e$			
RSFP	4.2×10^{-4}	7.9×10^{-9}	66.1	83%
NRSFP	119	4.0×10^{-9}	66.4	82%
LMA	0.47	5.6×10^{-5}	68.0	78%
	$\mu_\nu B\neq 0$ with SNO CC $\bar{\nu}_e$			
RSFP	5.3×10^{-4}	7.9×10^{-9}	65.8	84%
NRSFP	3×10^{3}	4.0×10^{-9}	66.4	82%
LMA	0.47	5.6×10^{-5}	68.1	78%

III. FIT PROCEDURE

Global analyzes of solar neutrino data have become quite standard; for a recent reference see [9]. Here we briefly describe the main features of our analysis.

In order to determine the expected event numbers for the various solar neutrino experiments we calculate the ν_e survival probability for each point in parameter space. We adopt standard solar model neutrino fluxes [31], treating, however, the ^{8}B neutrino flux normalization as a free parameter f_B, which is constrained by the SNO NC measurement. In order to determine the expected signal in each detector, these fluxes are convoluted with the survival probability at the detector, the neutrino cross sections and the detector response functions for Super-Kamiokande [3] and SNO [33]. We use the efficiencies employed previously, e.g., in Ref. [9]. For the SNO case the charged current and NC cross sections of neutrinos on deuterium were taken from Ref. [34] and the response functions from [33].

We also include theoretical and experimental errors and their cross correlations, following the standard covariance

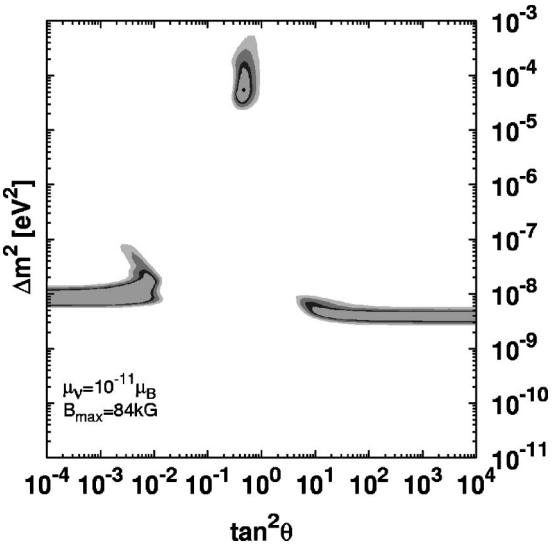

FIG. 3. Allowed regions of $\tan^2\theta_{SOL}$ and Δm^2_{SOL} for the two-flavor spin flavor precession solutions RSFP and NRSFP as well as the LMA oscillation solution.

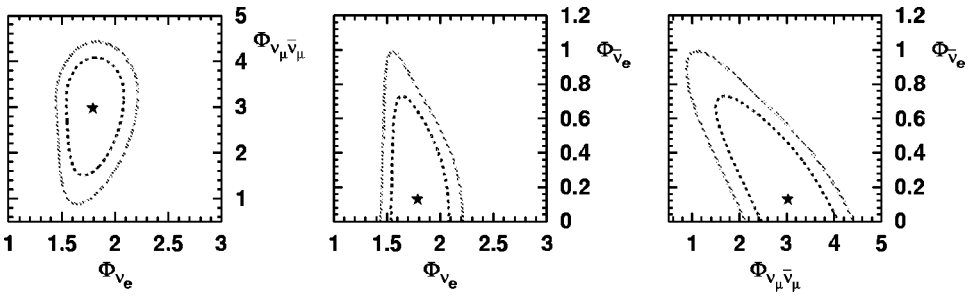

FIG. 4. Solar neutrinos fluxes Φ_{ν_e}, $\Phi_{\nu_\mu\bar{\nu}_\mu}=\Phi_{\nu_\mu}+\Phi_{\bar{\nu}_\mu}$, and $\Phi_{\bar{\nu}_e}$ (in units of 10^6 cm^{-2} s^{-1}) derived from the number of events per bin at SNO for an undistorted ^{8}B spectrum.

approach. In particular, the errors associated with the energy-scale and the energy-resolution uncertainties of the Super-Kamiokande and SNO experiments are included.

Here we use all current solar neutrino data [4]: the solar neutrino rates of the chlorine experiment ($2.56\pm0.16\pm0.16$ SNU), the most recent gallium results SAGE ($70.8^{+5.3+3.7}_{-5.2-3.2}$ SNU) and GALLEX/GNO ($70.8\pm4.5\pm3.8$ SNU), as well as the 1496-day Super-Kamiokande data sample [3] in the form of 44 bins (eight energy bins, six of which are further divided into seven zenith angle bins). In addition to this, we include the latest results from SNO presented in Refs. [1,2], in the form of 34 data bins (17 energy bins for each day and night period).

Therefore we have in total $3+44+34=81$ observables in our statistical analysis, which we fit in terms of the parameters Δm^2_{SOL}, θ_{SOL}. The third parameter $\mu B_\perp$ characterizing the maximum magnitude of the magnetic field in the convective zone is fixed at its optimum value $B_\perp=84$ kG. As mentioned, we employ the self-consistent magnetohydrodynamics magnetic field profile obtained in Ref. [12] for $k=6$ and $R_0=0.6R_\odot$.

We have compared the data described above with the expected event numbers, taking into account the relevant detector characteristics and response functions. Using a suitable definition of χ^2_{SOL} (the same as in Ref. [9], except that we leave the boron flux free and remove the corresponding theoretical flux errors from the covariance matrix) we have performed a global fit of present solar neutrino data. The allowed regions for a given C.L. with two degrees of freedom (DOF) are defined as the set of points satisfying the condition

$$\chi^2_{\rm SOL}(\Delta m^2,\theta)-\chi^2_{\rm SOL,min}\leqslant\Delta\chi^2({\rm C.L.},2{\rm DOF}), \qquad (3)$$

where $\Delta\chi^2$(C.L.,DOF)$=4.61$, 5.99, 9.21, 11.83 for 90%, 95%, 99% C.L. and 3σ, respectively.

We present in Fig. 3 the allowed regions of $\tan^2\theta_{SOL}$ and Δm^2_{SOL} for the two-flavor spin flavor precession. The confidence levels are 90%, 95%, 99%, and 3σ for two DOF. As noted previously, we reconfirm the appearance of two new solutions, totally due to the effect of the magnetic field. The first is the RSFP solution [12], which extends up to $\tan^2\theta$ values around 10^{-2} or so. In addition, one finds a nonresonant (NRSFP) solution [11] in the ''dark side'' of parameter space, for large $\tan^2\theta$ values. The fits corresponding to these two spin flavor precession solutions are slightly better than that for the LMA solution, which is recovered without any essential change due to the effect of the magnetic moment. Note, however, that the contours are defined with respect to the global minimum of χ^2, and that this is located at the RSFP solution. As a result the LMA region in our case is slightly smaller than the one corresponding to the pure oscillation case (no magnetic field) [9].[2]

A characteristic feature of spin flavor precession solutions is that they produce electron antineutrinos, in contrast with the oscillation case. One of the new features of our present results is that, in contrast to what was found previously [11,12], the solar data alone are now sufficient to rule out all oscillation solutions other than the LMA, without need to include as part of our χ^2_{SOL} the term corresponding to the data of the LSD experiment [35] or the electron antineutrino Super-K flux limits [29]. While the inclusion of these terms would reduce the two SFP branches, in this paper we will show how the solar neutrino data sample including the solar antineutrino rates at SNO leads to the same effect. Before we do that, let us first generalize the neutral and charged flux

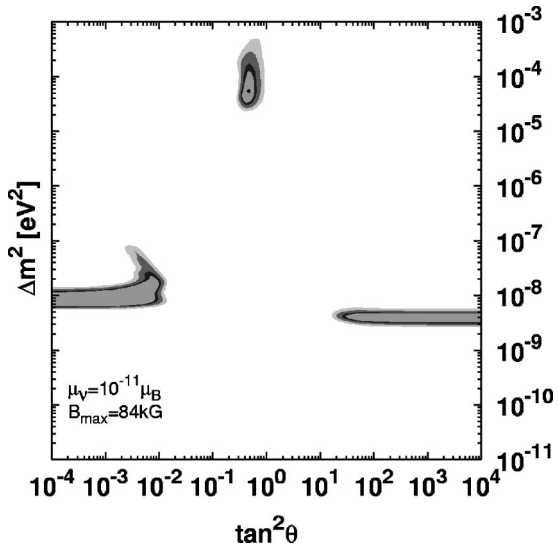

FIG. 5. Same plot as in Fig. 3, but including the electron antineutrino CC interaction in SNO ($\bar{\nu}_e+D\to n+n+e^+$) with the approximation discussed in text.

[2]In Fig. 3 we have adjusted the value of $\mu B_\perp$ to its best value (for $\mu=10^{-11}\mu_B$ this corresponds to a maximum magnetic field $B_\perp=84$ kG).

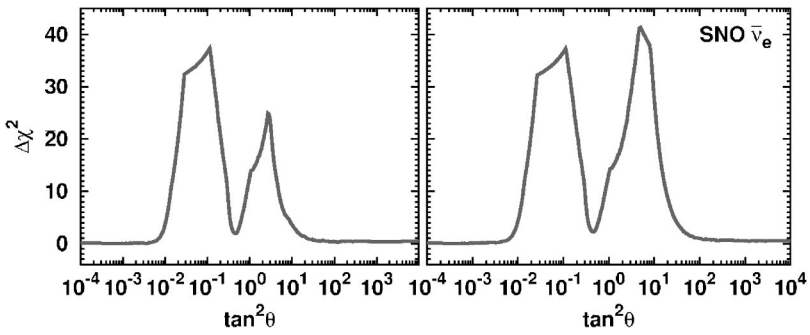

FIG. 6. $\Delta\chi^2_{SOL}$ as a function of $\tan^2\theta$ with respect to the favored spin flavor precession solution.

discussion given by SNO [1] to the case where there is also a third flux, namely, that of solar antineutrinos, expected in the SFP scenario.

In Fig. 4 we display the solar neutrinos fluxes including the electron-antineutrino flux, namely, Φ_{ν_e}, $\Phi_{\nu_\mu\bar{\nu}_\mu}=\Phi_{\nu_\mu}+\Phi_{\bar{\nu}_\mu}$, and $\Phi_{\bar{\nu}_e}$ as derived from the observed SNO event number, assuming an undistorted ^{8}B spectrum. Note that fluxes are in units of 10^6 cm^{-2} s^{-1} and that here we assume the standard solar model (SSM) boron flux prediction.

In the left panel we give the muon neutrino flux versus the electron neutrino flux. The middle and right panels give the electron antineutrino flux versus the electron neutrino flux (middle) and versus the muon-type neutrino flux (right). These contours correspond to 68% C.L. and 90% C.L. for two DOF. One sees that the electron antineutrino flux, calculated with the cross sections in [34], is constrained in model-independent way to be less than 1×10^6 cm^{-2} s^{-1} at 90% C.L. The best fitted fluxes are: $\Phi_{\nu_e}=1.79\times10^6$ cm^{-2} s^{-1}, $\Phi_{\nu_\mu\bar{\nu}_\mu}=3.02\times10^6$ cm^{-2} s^{-1}, $\Phi_{\bar{\nu}_e}=0.14\times10^6$ cm^{-2} s^{-1}, with $\chi^2_{\min}=16.7$ and 15 DOF. Note that the best fit flux $\Phi_{\bar{\nu}_e}$ shown by stars in Fig. 4 is compatible with zero at 97% C.L.

Encouraged by the consistency of our generalization of the SNO procedure for the SFP case, we now move to the inclusion of the antineutrino data in the analysis. The reaction $\bar{\nu}_e+D\rightarrow n+n+e^+$ would lead, in addition to the positron Cerenkov light, to the capture of two neutrons by deuteron(s) and the production of two monochromatic gammas with energy $E_\gamma\approx6.25$ MeV. Clearly, a complete analysis of the associated signal arising from this cannot be performed at the moment, since we lack the appropriate response function.[3] As an approximation we can, however, assume that the positron resolution function is the same as for electrons, and also that the two neutrons can be captured by deuteron in the same way as the neutrons in the NC channel (this last contribution is the most important one). Under this approximation we obtain in Fig. 5 an estimate of the allowed regions. Particularly noticeable is the fact that in this case the dark side region becomes smaller. This cut is required in order to avoid an unacceptably high solar antineutrino flux (above 20% or so of the boron-8 neutrino flux) for values of $\tan^2\theta\lesssim20$. This exercise highlights the relevance of solar antineutrino searches at SNO in restricting the parameter space of SFP solutions. This possibility using Super-K is certainly less favorable.

Before we conclude this section let us present in Table I the goodness of fit (GOF) corresponding to each of our three solutions. The analysis has been done for 81 (chlorine+GNO+SAGE+Zenith SK spectrum+SNO D/N spectrum)-3 parameters: $\tan^2\theta_{SOL}$, Δm^2_{SOL}, and the boron flux f_B, corresponding to 78 DOF. This table shows the best-fit parameter values, $\chi^2_{\min}$ and GOF for the three solutions. The top panel refers to the usual oscillation case, the middle panel corresponds to the fit without including the SNO antineutrino CC interaction, and the bottom panel is for the case where this interaction is included.

To close this session we now illustrate more concisely the above results by displaying in Fig. 6 the profiles of $\Delta\chi^2_{SOL}$ as a function of $\tan^2\theta_{SOL}$. This is obtained by minimizing with respect to the undisplayed oscillation parameters, for the fixed $\mu B_\perp$ value indicated above. Note that the $\Delta\chi^2_{SOL}$ is calculated with respect to the favored spin flavor precession solution. The first thing to notice are the two *plateaus* corresponding to the RSFP and NRSFP solutions, slightly lower than the LMA $\chi^2_{\min}$. In contrast to the left panel, the right panel includes the electron antineutrino CC interaction in SNO. One can see how the NRSFP plateau has now become narrower (see also Fig. 5). Moreover, one can appreciate two very small kinks corresponding to the ''would-be'' LOW solutions. Their status worsens and their position shifts slightly toward the ''dark side.''

IV. FUTURE EXPERIMENTS

We have seen how the SFP scenario leads to three very good descriptions of current solar neutrino data corresponding to the RSFP, NSRFP, and LMA solutions. The issue arises as to how to distinguish between these solutions, which are presently statistically equivalent. Note that this is not such an easy task since, as seen in Fig. 2, the expected spectral energy distribution for our spin flavor precession solutions is hardly distinguishable from the one expected in the pure LMA oscillation solution. Moreover, in contrast to the oscillation solution, where a day-night effect is predicted, the SFP spectra show no day-night asymmetry.

There is at the moment great expectation as to the first physics results of the upcoming KamLAND experiment, expected shortly [36]. Here we analyze the implications of two

[3]We thank Art McDonald for useful discussions.

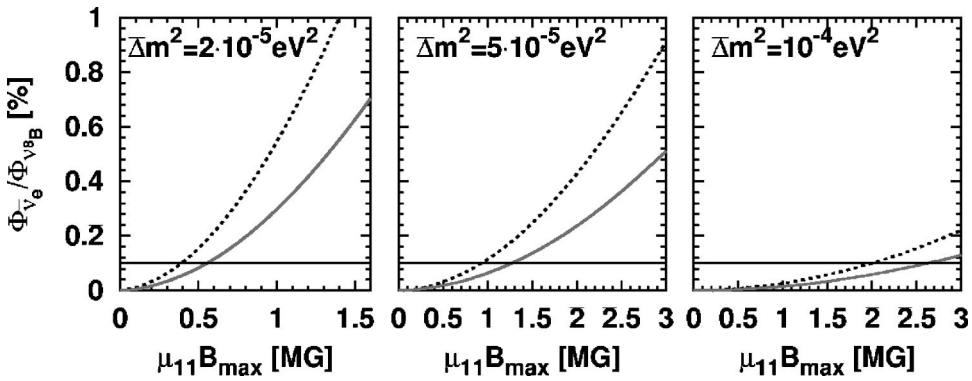

FIG. 7. KamLAND sensitivity to the Majorana neutrino transition magnetic moment in case the LMA solution is confirmed. See text.

possible outcomes of the KamLAND experiment for the status of SFP solutions.

A. If KamLAND confirms the LMA oscillation solution

In this case all alternative solutions, such as the present spin flavor precession solutions, may be present only at a subleading level and, on the basis of how good is the KamLAND determination of the LMA oscillation parameters, one will correspondingly constrain any exotic alternative. Our resulting constraints on the SFP solutions are illustrated in Fig. 7. In Fig. 7 we have displayed the electron antineutrino flux predicted at KamLAND ($E>8.3$ MeV) for three different Δm^2_{SOL} values (indicated in the figure) and for $\tan^2\theta_{SOL}$ values varying in the range from 0.3 to 0.8, as a function of $\mu_{11}B_{\max}$, μ_{11} being the magnetic moment in units of $10^{-11}\mu_B$ and $B_{\max}$ being the maximum magnetic field in the convective zone. In order to obtain such a simple correlation we note the importance of using our self-consistent magnetohydrodynamics magnetic field profile, as in Ref. [12]. The extremes of the neutrino mixing range correspond to the solid and dashed lines indicated in the figure, while the horizontal line corresponds to a KamLAND sensitivity to the antineutrino flux of 0.1%, expected with three years running [36]. Clearly the limits on the transition magnetic moments are sensitive also to the ultimate central Δm^2_{SOL} value indicated by KamLAND (a 10% error is expected), being more stringent for lower Δm^2_{SOL} values, as seen from the left panel.

B. If KamLAND does not confirm the LMA solution

Imagine now the extreme and unlikely case that KamLAND does not provide useful information on the neutrino parameters. In this case one can compare the predictions of these three solutions for the upcoming Borexino experiment, as suggested in Ref. [37].

A simple way to display this is presented in Fig. 8. This figure shows the predicted values for

$$R_{\rm Borexino} \equiv \text{observed Borexino rate} \;\; \text{SSM rate}, \qquad (4)$$

defined as the ratio of the observed-over-SSM-expected signal in Borexino, assuming best-fit parameters as determined in our fit, and 90% C.L. error bars for LMA (left line), RSFP (middle lines), and NRSFP (right lines) solutions. For the SFP solutions two error bars are indicated for $R_{\rm Borexino}$. The error bars indicated in gray refers to the cases $\theta=0$ for the RSFP case and $\theta=\pi/2$ for the NRSFP solution. The error bars indicated in black correspond to the general SFP case with nonzero mixing. Clearly, the zero mixing RSFP and the LMA solutions lead to very different predictions, as already

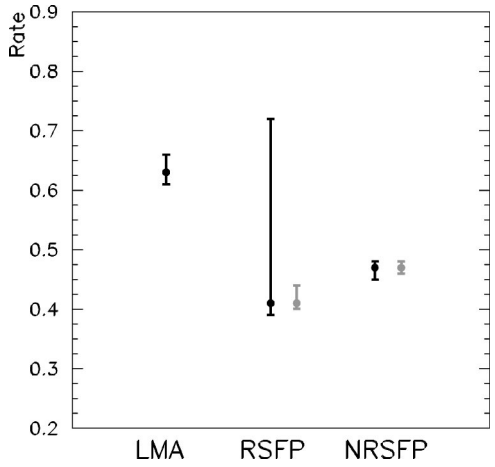

FIG. 8. Predicted $R_{\rm Borexino}$ values for LMA and spin flavor precession solutions.

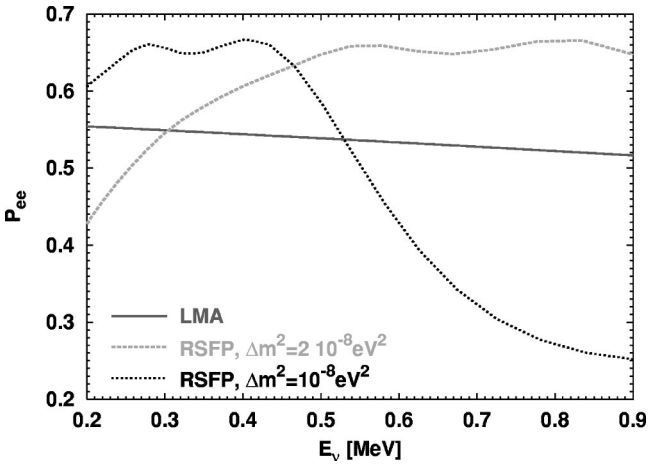

FIG. 9. Neutrino survival probability for RSFP-like solution with $\Delta m^2_{SOL}\sim 2\times10^{-8}$ eV^2 and $\tan^2\theta_{SOL}\sim10^{-2}$, in the range between 0.2 and 0.9 MeV.

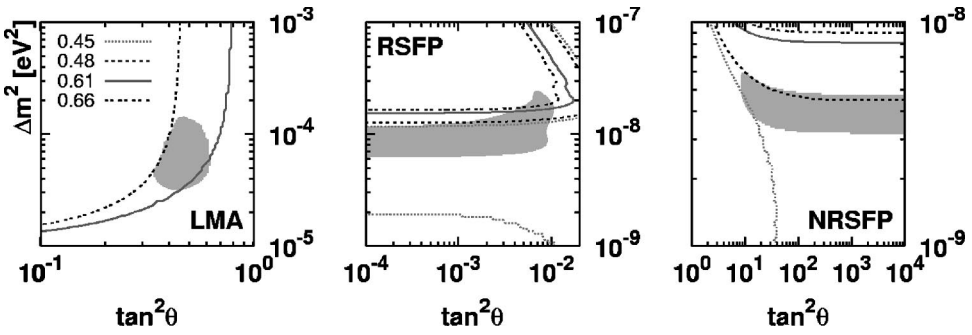

FIG. 10. Contour lines of predicted R_{Borexino} values as a function of the neutrino oscillation parameters. The shaded regions correspond to the three solutions discussed here (LMA, left panel), RSFP (middle panel), and NRSFP (right panel). See text.

noted in Ref. [37]. However, we remark that in general the RSFP solution cannot be distinguished from LMA insofar as the Borexino predition is concerned. Indeed, as seen from Fig. 6, the RSFP solution is characterized by a very flat plateau of nearly constant χ^2, while the Borexino prediction depends rather strongly on the poorly determined value of the ''best'' neutrino mixing angle for this solution. To see this let us take, for example, $\Delta m^2_{SOL} \sim 2\times 10^{-8}$ eV^2 and $\tan^2\theta_{SOL} \sim 10^{-2}$, and display the neutrino survival probability versus energy, as seen in Fig. 9. One sees from this figure how in the *pp* region this solution is similar to LMA, but leads to a much smaller suppression of the beryllium line. This allows us to understand the inability to predict with precision the borexino rate expected in this part of the (lowest) RSFP region. In contrast, the NRSFP solution in the ''dark side'' is the one that is more clearly distinguishable from the LMA oscillation solution. Moreover, we have verified that, for the case of the NRSFP solution, the Borexino predition is rather insensitive to whether the neutrino mixing is left free or not.

A more complete way to present this information is displayed in Fig. 10. Here we have overlapped the allowed neutrino parameter ranges determined from our fit with the predicted R_{Borexino} values, for each one of these solutions, RSFP, NRSFP, and LMA, at 90% C.L. The results for the LMA solution agree well with those obtained, say, in Refs. [21,24]. We can clearly identify from Fig. 10 which range in the 90% allowed confidence RSFP region leads to the large ''spread'' in the Borexino prediction discussed previously.

V. SUMMARY AND DISCUSSION

In this paper we have reconsidered the solutions of the solar neutrino problem involving two-flavor oscillations and spin flavor precessions. We have given a global analysis of such SFP solutions to the solar neutrino problem, taking into account the impact of the full set of latest solar neutrino data, including the recent SNO data as well as the 1496-day Super-Kamiokande data. These are characterized by three effective parameters: $\Delta m^2_{SOL} \equiv \Delta m^2$, the neutrino mixing angle $\theta_{SOL} \equiv \theta$, and the magnetic field parameter $\mu B_\perp$. For the last we have fixed $\mu = 10^{-11}\mu_B$, with a corresponding optimized self-consistent magnetohydrodynamics magnetic field profile with $B_\perp \sim 80$ kG as the maximum field strength in the convective zone. Two-flavor oscillations are recovered as a particular case of our general SFP scenario. We have found that no LOW quasivacuum or vacuum solutions are present at the 3σ level. In addition to the standard LMA oscillation solution, we have reconfirmed the existence of two SFP solutions, in the resonant (RSFP) and nonresonant (NRSFP) regimes. These two SFP solutions have goodness of fit of 84% (RSFP) and 83% (NRSFP), slightly better than that of the LMA oscillation solution (78%). We have discussed the role of solar antineutrino searches in the fit and present a table of best-fit parameters and χ^2_{min} values. Should KamLAND confirm the LMA solution, the SFP solutions may at best be present at a subleading level, leading to a meaningful constraint on $\mu B_\perp$. If the magnetic field strength is known from solar physics, we can obtain a bound on the Majorana neutrino transition magnetic moment, complementary to the bounds discussed in Ref. [30]. In the event LMA is not the solution realized in nature, then future experiments such as Borexino can be of help in distinguishing LMA from the NRSFP solution, as well as the restricted RSFP solution with no mixing.

ACKNOWLEDGMENT

We would like to thank E. Akhmedov, Michele Maltoni, and Mariam Tórtola for useful discussions and K. Kubodera, for providing antineutrino-deuteron cross sections. This work was supported by Spanish grant PB98-0693, by the European Commission RTN network HPRN-CT-2000-00148, by the European Science Foundation network Grant No. 86, by the Iberdrola Foundation (V.B.S.) and by an INTAS grant YSF 2001/2-148 and CSIC-RAS agreement (T.I.R.). V.B.S. and T.I.R. were partially supported by the RFBR grant 00-02-16271 and O.G.M. was supported by the CONACyT-Mexico grants J32220-E and 35792-E.

[1] SNO Collaboration, Q. R. Ahmad *et al.*, Phys. Rev. Lett. **89**, 011301 (2002).

[2] SNO Collaboration, Q. R. Ahmad *et al.*, Phys. Rev. Lett. **89**, 011302 (2002).

[3] Super-Kamiokande Collaboration, S. Fukuda *et al.*, Phys. Lett. B **539**, 179 (2002).

[4] B. T. Cleveland *et al.*, Astrophys. J. **496**, 505 (1998); Kamiokande Collaboration, Y. Fukuda *et al.*, Phys. Rev. Lett. **77**,

1683 (1996); GALLEX Collaboration, W. Hampel *et al.*, Phys. Lett. B **447**, 127 (1999); SAGE Collaboration, D. N. Abdurashitov *et al.*, Phys. Rev. Lett. **83**, 4686 (1999); Phys. Rev. C **60**, 055801 (1999); SAGE Collaboration, J. N. Abdurashitov *et al.*, astro-ph/0204245; GNO Collaboration, M. Altmann *et al.*, Phys. Lett. B **490**, 16 (2000); GNO Collaboration, E. Bellotti *et al.*, Nucl. Phys. B (Proc. Suppl.) **91**, 44 (2001); Super-Kamiokande Collaboration, Y. Fukuda *et al.*, Phys. Rev. Lett. **81**, 1158 (1998); **81**, 4279(E) (1998); **82**, 1810 (1999); Super-Kamiokande Collaboration, Y. Suzuki, Nucl. Phys. B (Proc. Suppl.) **91**, 29 (2001); Super-Kamiokande Collaboration, S. Fukuda *et al.*, Phys. Rev. Lett. **86**, 5651 (2001); SNO Collaboration, Q. R. Ahmad *et al.*, *ibid.* **87**, 071301 (2001).

[5] See, for example, N. Fornengo, M. C. Gonzalez-Garcia, and J. W. Valle, Nucl. Phys. **B580**, 58 (2000).

[6] CHOOZ Collaboration, M. Apollonio *et al.*, Phys. Lett. B **466**, 415 (1999); Palo Verde Collaboration, F. Boehm *et al.*, Phys. Rev. D **64**, 112001 (2001).

[7] N. Fornengo, M. Maltoni, R. T. Bayo, and J. W. Valle, Phys. Rev. D **65**, 013010 (2002).

[8] M. C. Gonzalez-Garcia, M. Maltoni, C. Pena-Garay, and J. W. F. Valle, Phys. Rev. D **63**, 033005 (2001); G. L. Fogli, in Neutrino Telescopes 2001, Venice, Italy, 2001.

[9] M. Maltoni, T. Schwetz, M. A. Tortola, and J. W. Valle, hep-ph/0207227.

[10] M. Guzzo *et al.*, Nucl. Phys. **B629**, 479 (2002).

[11] O. G. Miranda, C. Pena-Garay, T. I. Rashba, V. B. Semikoz, and J. W. Valle, Phys. Lett. B **521**, 299 (2001).

[12] O. G. Miranda, C. Pena-Garay, T. I. Rashba, V. B. Semikoz, and J. W. F. Valle, Nucl. Phys. **B595**, 360 (2001).

[13] E. K. Akhmedov and J. Pulido, Phys. Lett. B **485**, 178 (2000).

[14] M. M. Guzzo and H. Nunokawa, Astropart. Phys. **12**, 87 (1999); H. Nunokawa and H. Minakata, Phys. Lett. B **314**, 371 (1993).

[15] J. Derkaoui and Y. Tayalati, Astropart. Phys. **14**, 351 (2001).

[16] J. Schechter and J. W. F. Valle, Phys. Rev. D **24**, 1883 (1981); **25**, 283(E) (1982).

[17] E. K. Akhmedov, Phys. Lett. B **213**, 64 (1988); C. Lim and W. J. Marciano, Phys. Rev. D **37**, 1368 (1988).

[18] J. Schechter and J. W. F. Valle, Phys. Rev. D **22**, 2227 (1980).

[19] V. A. Kutvitskii and L. S. Solov'ev, Sov. Phys. JETP **78**, 456 (1994).

[20] M. C. Gonzalez-Garcia, P. C. de Holanda, C. Pena-Garay, and J. W. Valle, Nucl. Phys. **B573**, 3 (2000), and references therein.

[21] J. N. Bahcall, M. C. Gonzalez-Garcia, and C. Pena-Garay, J. High Energy Phys. **07**, 054 (2002).

[22] A. Bandyopadhyay, S. Choubey, S. Goswami, and D. P. Roy, Phys. Lett. B **540**, 14 (2002).

[23] V. Barger, D. Marfatia, K. Whisnant, and B. P. Wood, Phys. Lett. B **537**, 179 (2002).

[24] P. C. de Holanda and A. Y. Smirnov, hep-ph/0205241.

[25] A. Strumia, C. Cattadori, N. Ferrari, and F. Vissani, Phys. Lett. B **541**, 327 (2002).

[26] G. L. Fogli, E. Lisi, A. Marrone, D. Montanino, and A. Palazzo, Phys. Rev. D **66**, 053010 (2002).

[27] R. Barbieri, G. Fiorentini, G. Mezzorani, and M. Moretti, Phys. Lett. B **259**, 119 (1991).

[28] P. Vogel and J. F. Beacom, Phys. Rev. D **60**, 053003 (1999).

[29] M. B. Smy (private communication); C. Yanagisawa, talk given at the Euroconference on Frontiers on Cosmology and Astroparticle Physics, Saint Feliu de Guixols, Spain, Proceedings Supplements, 2001, Vol. 95.

[30] W. Grimus *et al.*, hep-ph/0208132, and references therein.

[31] http://www.sns.ias.edu/~jnb/SNdata/Export/BP2000; J. N. Bahcall, S. Basu, and M. H. Pinsonneault, Astrophys. J. **529**, 1084 (2000); **555**, 990 (2001).

[32] A. M. Dziewonski and D. L. Anderson, Phys. Earth Planet. Inter. **25**, 297 (1981).

[33] SNO Collaboration, http://www.sno.phy.queensu.ca/sno/prlwebpage/

[34] J. F. Beacom and S. J. Parke, Phys. Rev. D **64**, 091302 (2001); S. Nakamura, T. Sato, V. Gudkov, and K. Kubodera, Phys. Rev. C **63**, 034617 (2001); M. Butler, J.-W. Chen, and X. Kong, *ibid.* **63**, 035501 (2001); I. S. Towner, *ibid.* **58**, 1288 (1998); S. Nakamura, T. Sato, S. Ando, T. S. Park, F. Myhrer, V. Gudkov, and K. Kubodera, Nucl. Phys. **A707**, 561 (2002); http://www-nuclth.phys.sci.osaka-u.ac.jp/users/nakamura/research/index.html

[35] M. Aglietta *et al.*, Pis'ma Zh. Éksp. Teor. Fiz. **63**, 753 (1996) [JETP Lett. **63**, 791 (1996)].

[36] A. Piepke, Nucl. Phys. B (Proc. Suppl.) **91**, 99 (2001); http://kamland.lbl.gov/KamLAND

[37] E. K. Akhmedov and J. Pulido, Phys. Lett. B **529**, 193 (2002).